Rapid Communications

Interband π-like plasmon in silicene grown on silver

A. Sindona,[1,2,*] A. Cupolillo,[1,2,†] F. Alessandro,[1] M. Pisarra,[3] D. C. Coello Fiallos,[1] S. M. Osman,[1] and L. S. Caputi[1]

[1]*Dipartimento di Fisica, Università della Calabria, Via P. Bucci, Cubo 30C, I-87036 Rende (CS), Italy*

[2]*INFN, Sezione LNF, Gruppo Collegato di Cosenza, Cubo 31C, I-87036 Rende (CS), Italy*

[3]*Departamento de Química, Universidad Autónoma de Madrid, Calle de Francisco Tomás y Valiente 7, E-28049 Madrid, Spain*

(Received 13 August 2017; revised manuscript received 6 December 2017; published 3 January 2018)

Silicene, the two-dimensional allotrope of silicon, is predicted to exist in a low-buckled honeycomb lattice, characterized by semimetallic electronic bands with graphenelike energy-momentum dispersions around the Fermi level (represented by touching Dirac cones). Single layers of silicene are mostly synthesized by depositing silicon on top of silver, where, however, the different phases observed to date are so strongly hybridized with the substrate that not only the Dirac cones, but also the whole valence and conduction states of ideal silicene appear to be lost. Here, we provide evidence that at least part of this semimetallic behavior is preserved by the coexistence of more silicene phases, epitaxially grown on Ag(111). In particular, we combine electron energy loss spectroscopy and time-dependent density functional theory to characterize the low-energy plasmon of a multiphase-silicene/Ag(111) sample, prepared at controlled silicon coverage and growth temperature. We find that this mode survives the interaction with the substrate, being perfectly matched with the π-like plasmon of ideal silicene. We therefore suggest that the weakened interaction of multiphase silicene with the substrate may provide a unique platform with the potential to develop different applications based on two-dimensional silicon systems.

DOI: 10.1103/PhysRevB.97.041401

Following the isolation of graphene sheets by mechanical exfoliation of its parent crystal graphite [1], enormous effort has been directed towards two-dimensional (2D) crystals made of group-IV elements other than carbon.

A particularly noteworthy example is silicene, the silicon equivalent of graphene with a natural compatibility with current semiconductor technology [2–4]. First-principles calculations of the structural properties report an intrinsic stability of a honeycomb arrangement of Si atoms in slightly buckled form, with mixed sp^2-sp^3 hybridization [5–7]. This system, referred to as freestanding or (1×1) silicene, presents a graphenelike, semimetallic electronic structure characterized by linearly dispersing π and π^* bands around the Fermi energy E_F, thus effectively allowing the charge carriers to mimic massless relativistic particles [8,9]. Unlike graphene, freestanding silicene has a large spin-orbit coupling, which would make it suitable for valley-spintronic applications [10,11], and an electrically, magnetically, or chemically tunable band gap [12–17], which would be crucial for engineering on-off current ratios and charge-carrier mobility in silicene field-effect transistors.

On the practical side, silicenelike nanostructures are synthesized by the epitaxial growth [18,19] of silicon on silver [20–26] and a few other metal substrates [27,28], very recently including gold [29]. In particular, a number of well-ordered domains have been observed on Ag(111), the formation and coexistence of which depend on the substrate temperature, during silicon growth, and the silicon deposition rate [30–36].

Most of these domains have a crystalline morphology that is closely commensurate with the (4×4), $(2\sqrt{3}\times2\sqrt{3})R30^\circ$, and $(\sqrt{13}\times\sqrt{13})R13.9^\circ$ phases [34–46] of Fig. 1. The different orientation, out-of-plane atomic buckling, and lattice constant of the Si atoms in these superstructures, here denoted (3×3), $(\sqrt{7}\times\sqrt{7})_{\rm I}$, and $(\sqrt{7}\times\sqrt{7})_{\rm II}$, are reflected in markedly distinct electronic properties of the silicene overlayers that, even without the supporting Ag substrate below, may or may not preserve the Dirac cones of (1×1) silicene [33,34,47,48]. Other phases and more complex scenarios, including silicon-induced faceting, are reported in the literature [26,33,37,47,49,50].

As for the interaction with Ag(111), silicene seems to lose the unique properties of its (1×1) form, as confirmed by angle-resolved photoemission spectroscopy (ARPES) measurements combined with density functional calculations [51–56]. Indeed, the initial evidence of Dirac cones in the (4×4) phase [25,36] has been reinterpreted as originating from the s and p states of bulk Ag, or the strongly hybridized sp states of Ag and Si [56]. More recent developments [57] suggest that a hybridized Dirac-cone structure is unusually formed, as a result of the aforementioned hybridization. Even in this latter case, however, the π-like bands of freestanding silicene are destroyed by its interaction with Ag. Thus, contrary to well-consolidated technologies of graphene growth on copper, the transfer of silicene to other substrates appears impractical.

The intercalation of alkali-metal atoms between silicene and Ag(111) is predicted to effectively restore the Dirac cones [58]. Another possibility has been indicated by changing the supporting substrate to Au(111) [29]. Nonetheless, the major goal of silicene technology is still to grow a honeycomblike

*antonello.sindona@fis.unical.it

†anna.cupolillo@fis.unical.it

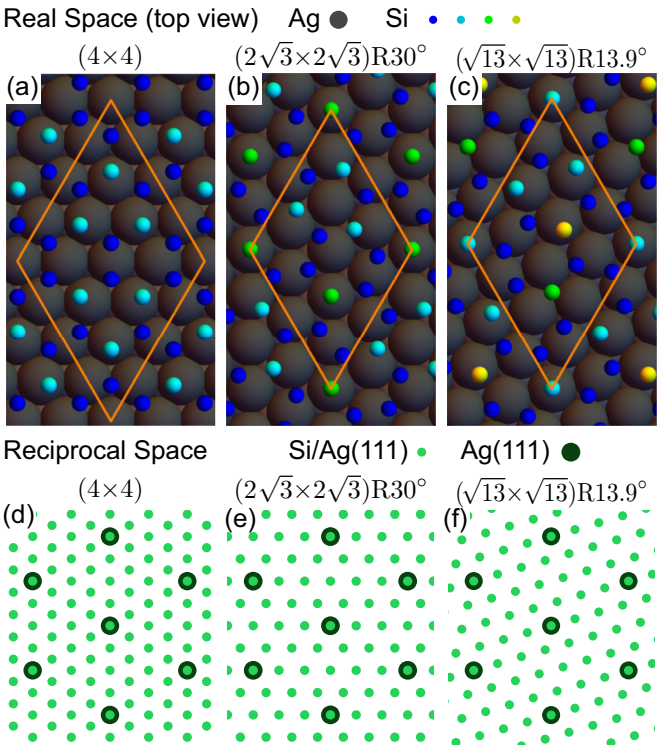

Silicene overlayer

Si/Ag phase	(4×4)	$(2\sqrt{3}\times2\sqrt{3})R30°$	$(\sqrt{13}\times\sqrt{13})R13.9°$
Si supercell	(3×3)	$(\sqrt{7}\times\sqrt{7})_{I}$	$(\sqrt{7}\times\sqrt{7})_{II}$
$d_{Si\text{-}Si}$(Å)	2.17	2.18	2.25
$d_{Si\text{-}Ag}$(Å)	2.13	2.16	2.13
Δ_1(Å)	0.78	0.36	0.36
Δ_2(Å)		1.19	0.59
Δ_3(Å)			0.79

FIG. 1. Real and reciprocal spaces of the (4×4), $(2\sqrt{3}\times2\sqrt{3})R30°$, and one of the two inequivalent $(\sqrt{13}\times\sqrt{13})R13.9°$ phases of silicene on silver [33,35,36]. The unit cells of the superstructures are delimited by orange lines. The main geometric parameters of the silicene overlayers (commensurate supercell, average in-plane bond length $d_{Si\text{-}Si}$, minimum Si-Ag distance $d_{Si\text{-}Ag}$, and out-of-plane atomic buckling Δ_i) are derived from Refs. [47,48].

structure of Si atoms with semimetallic, π-like electronic features.

A different possible direction is outlined here, where, rather than looking at the band structure of silicene on Ag(111), we consider exploring the intrinsic plasmonics of the interface, i.e., the coherent charge-density oscillations of its valence electrons (plasmons). Specifically, we present low-energy electron diffraction (LEED) and electron energy loss spectroscopy (EELS) characterizations of two surface reconstructions of silicene on Ag(111), being, respectively, given by the $(2\sqrt{3}\times2\sqrt{3})R30°$ and a mixture of the (4 × 4), $(2\sqrt{3}\times2\sqrt{3})R30°$, and $(\sqrt{13}\times\sqrt{13})R13.9°$ superstructures. We report a clear signature of the existence of π and π^* states of silicene in the mixed phase, which reflects in a π-like plasmon structure detected in the energy loss (EL) spectrum of the system, alongside the Ag plasmon.

The measurements are consistent with time-dependent (TD) density functional theory (DFT) (TDDFT) calculations of the EL function of (1 × 1) silicene [59], showing a well-resolved loss peak at 1.75 eV for a momentum transfer of the order of 10^{-2} Å^{-1}. Furthermore, our results indicate that at least part of the π or π^* character of the first valence band (VB) or first conduction band (CB) of silicene grown on Ag(111) may be maintained under specific geometric conditions.

On the other hand, the π-like mode is absent in each single pure phase of the above-mentioned types, thus confirming that the semimetallic character of freestanding silicene is lost in favor of a hybridized band structure.

To begin, the experiments were carried out at room temperature in an ultrahigh vacuum chamber (with a base pressure of 2×10^{-10} Torr), using a high-resolution electron energy loss (EEL) spectrometer, equipped with two 50-mm hemispherical deflectors, as both monochromator and analyzer.

The EL spectra were acquired with an incident electron beam, about 0.2 mm wide, positioned at a fixed angle of 45° from the surface normal. The kinetic energy of the incident electrons was 40 eV. Scattered electrons were collected at an angle of 46° from the surface normal, with an overall energy resolution of 20 meV and an angular acceptance of 2°.

The silver substrate (a disk of about 8 mm diameter) was cleaned through several cycles of sputtering with 1 keV Ar^+ ions, at an operating pressure of 5×10^{-5} Torr, followed by annealing at 500 °C until a sharp LEED pattern showed the achievement of a clean and well-ordered Ag(111) surface.

Silicon was deposited on Ag(111) by thermal evaporation from a pure source, which was *slab cut* from a silicon wafer, clamped between two electrodes, and heated up, by passing a direct current thorough it, to obtain a stable vapor flux. During deposition, the silicon source was placed in front of the silver substrate, which was maintained at a constant temperature, controlled by a thermocouple placed close to the sample. The pressure during growth was less than 2×10^{-9} Torr. The uptake of Si was monitored by x-ray photoelectron spectroscopy and LEED.

Figure 2(a) shows the diffraction pattern acquired with the Ag substrate kept at 300 °C, during Si deposition. The LEED spots from this first sample are consistent with the reciprocal space points of Fig. 1(e), also reported in Fig. 2(c). Accordingly, they are readily interpreted as originating from a sufficiently *pure* $(2\sqrt{3}\times2\sqrt{3})R30°$ phase, in agreement with several previous studies [30,31,41–43]. On the other hand, the LEED image of Fig. 2(b) was acquired with the Ag substrate kept at 270 °C, during Si deposition. This second sample is characterized by a mixture of the (4 × 4), $(2\sqrt{3}\times2\sqrt{3})R30°$, and $(\sqrt{13}\times\sqrt{13})R13.9°$ phases. The possible formation of recently isolated multilayer silicene can be ruled out, because it would provide a different LEED pattern [51].

Indeed, the LEED spots from the second sample are in line with the reciprocal space points of the three phases, reported in Fig. 2(c), where the silicene superstructures are assumed to be perfectly matched with the Ag substrate. Interestingly, a visual inspection of Figs. 2(b) and 2(c) suggests a lattice mismatch of the $(\sqrt{7}\times\sqrt{7})_{I}$ and $(\sqrt{7}\times\sqrt{7})_{II}$ overlayers of ∼1% and ∼5%, respectively. Similar patterns, mostly concerning the

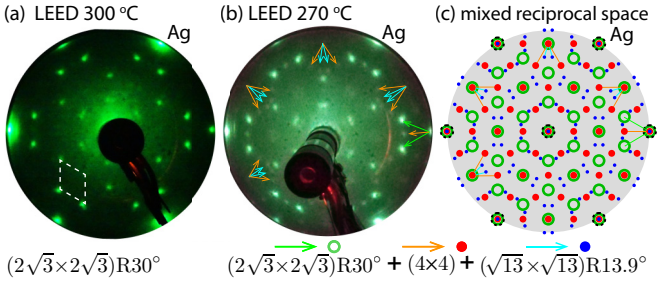

FIG. 2. LEED patterns of (a) the $(2\sqrt{3}\times2\sqrt{3})R30°$ phase and (b) the $(4\times4)+(2\sqrt{3}\times2\sqrt{3})R30°+(\sqrt{13}\times\sqrt{13})R13.9°$ phase of silicene on Ag(111). The coexistence of multiple domains in (b) is attested by spots of different intensity, being consistent with the mixed reciprocal space representation in (c). The latter includes the reciprocal space points of Figs. 1(d)–1(f), plus the reciprocal structure of the other $(\sqrt{13}\times\sqrt{13})R13.9°$ phase [33,35,36] not reported in Fig. 1.

(4×4) and $(\sqrt{13}\times\sqrt{13})R13.9°$ phases, have been discussed elsewhere [18,30,43–45], nonetheless, our composite structure, presenting a dominant $(2\sqrt{3}\times2\sqrt{3})R30°$ phase, which coexists with the (4×4) and $(\sqrt{13}\times\sqrt{13})R13.9°$ phases has yet to be reported.

The EELS measurements were performed with the samples directly transferred in the ELL spectrometer, without breaking the vacuum, and kept at room temperature with a pressure below 2×10^{-10} Torr. Figure 3 shows the EL spectra, in the range of 0–6 eV, obtained from (i) clean Ag(111), (ii) the pure $(2\sqrt{3}\times2\sqrt{3})R30°$ phase with the LEED pattern of Fig. 2(a), and (iii) the mixed phase with the LEED pattern of Fig. 2(b).

A prominent feature at ∼3.8 eV, which corresponds to the surface plasmon of Ag(111), dominates all spectra. Besides,

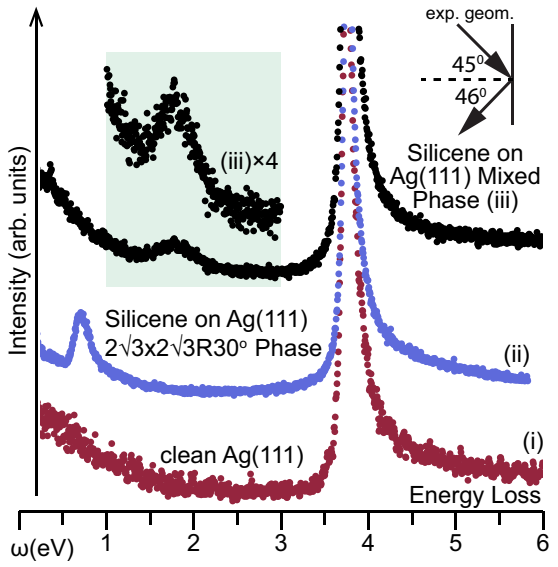

FIG. 3. EL spectra acquired, with a primary electron energy of 40 eV and the experimental geometry shown in the inset, from (i) clean Ag(111), (ii) silicene on Ag(111) in the pure $(2\sqrt{3}\times2\sqrt{3})R30°$ phase, and (iii) silicene on Ag(111) in the mixed $(4\times4)+(2\sqrt{3}\times2\sqrt{3})R30°+(\sqrt{13}\times\sqrt{13})R13.9°$ phase.

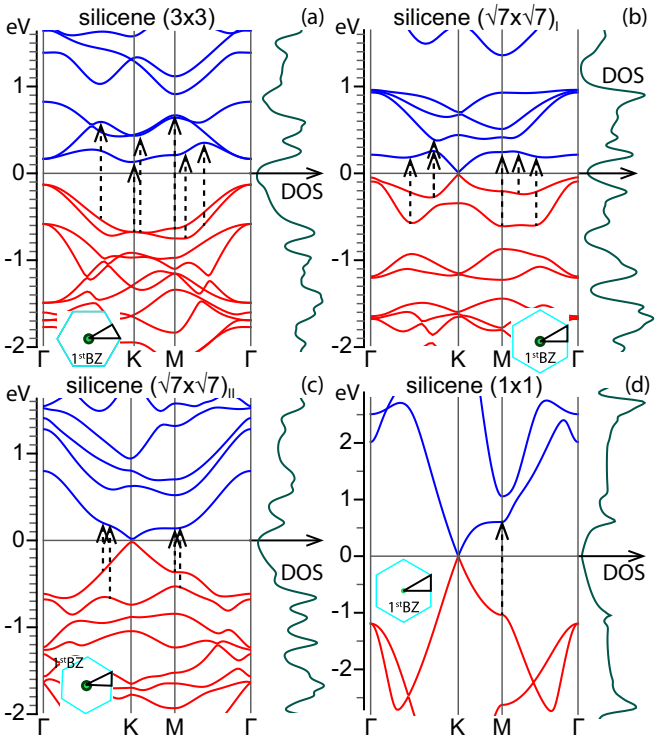

FIG. 4. Band structure (relative to $E_F=0$) and DOS for (3×3), $(\sqrt{7}\times\sqrt{7})_{\rm I}$, $(\sqrt{7}\times\sqrt{7})_{\rm II}$, and (1×1) silicene. The leading transitions concurring to the lower-energy loss peaks of Fig. 5 are represented by dashed arrow lines. The $\Gamma KM\Gamma$ paths of the superstructures are defined in the reciprocal spaces of Figs. 1(d)–1(f).

the Si/Ag(111) spectrum shows an additional loss at ∼0.7 eV in the pure phase and 1.75 eV in the mixed phase. The excitation energy of the former mode suggests the presence of a hybridized Si-Ag plasmon, whereas the latter mode resembles the π-like plasmon of (1×1) silicene [59].

To support this observation, we used TDDFT in the random phase approximation (RPA) and computed the dielectric properties of (1×1) silicene [59] in comparison with the (3×3), $(\sqrt{7}\times\sqrt{7})_{\rm I}$, and $(\sqrt{7}\times\sqrt{7})_{\rm II}$ overlayers of silicene, peeled from the silver substrate, in the (4×4), $(2\sqrt{3}\times2\sqrt{3})R30°$, and $(\sqrt{13}\times\sqrt{13})R13.9°$ phases of Fig. 1. These superstructures represent instructive examples of monolayer silicene, which, without the Ag substrate below, would not [Fig. 4(a)] and would [Figs. 4(b) and 4(c)] preserve the Dirac cones [33,34,47,48].

As it is customary in TDDFT [60], we started with a calculation of the ground-state electronic properties of the silicene systems by DFT [61] in the Kohn-Sham (KS) approach [62], using the generalized gradient approximation [63] and eliminating the core electrons by suitable norm-conserving pseudopotentials [64]. We selected a plane-wave (PW) basis set normalized to the systems' volume Ω, within an energy cutoff of 25 hartree, to represent the KS electron states $|\nu\mathbf{k}\rangle$, associated with the band energies $\varepsilon_{\nu\mathbf{k}}$, being labeled by a band index ν and a wave vector $\mathbf{k}$ in the first Brillouin zone ($1^{\rm st}$BZ). The bulk geometry, inherent to PW-DFT, was generated by replicating the silicene slabs with an out-of-plane vacuum distance of 25 Å.

Geometry optimization was performed on unsupported (1×1) silicene, obtaining a lattice constant of 3.82 Å and a characteristic buckling of the AB type, specified by a buckling distance of 0.45 Å [59]. As for supported silicene, the substrate was simulated by four silver planes with the morphologies of Fig. 1, starting from a set of optimized parameters found in Refs. [47,48]. Then, the positions of all atoms in the silicene and topmost Ag layers were relaxed using a Γ-centered Monkhorst-Pack (MP) grid [65] of $12 \times 12 \times 1$ **k** points in the 1stBZ, with the occupied and the first few empty band states of the systems. Further details on the electronic features of the $(2\sqrt{3} \times 2\sqrt{3})R30^\circ$ phase are provided in Sec. A of the Supplemental Material [66].

Single-point self-consistent runs were carried out in the local density approximation (LDA) [67] on a finer MP mesh of $60 \times 60 \times 1$ **k** points, by removing the silver layers and keeping the same relaxed positions for the Si atoms as the geometry optimization step. Subsequently, the converged electron densities were used, in non-self-consistent runs, to obtain the eigensystem $(|\nu\mathbf{k}\rangle, \varepsilon_{\nu\mathbf{k}})$ on highly resolved grids of $240 \times 240 \times 1$ points for (1×1) silicene, $90 \times 90 \times 1$ points for (3×3) silicene, and $72 \times 72 \times 1$ points for the other two silicene superstructures [$(\sqrt{7} \times \sqrt{7})_{\mathrm{I}}$ and $(\sqrt{7} \times \sqrt{7})_{\mathrm{II}}$]. A number of empty bands covering the KS energy spectrum up to 15 eV, above E_F, was selected in all non-self-consistent cases, to accurately describe the systems' plasmonics at energy losses below 6 eV.

The electronic structure and density of states (DOS) of our DFT+LDA computations are reported in Fig. 4, with the band energies represented along the $\Gamma K M \Gamma$ paths of the corresponding reciprocal spaces (Fig. 1). Here, we spot some peculiar features partly recognized in previous studies [47,48,59].

(3×3) silicene has no Dirac cones at K and presents a direct gap at Γ of ~0.3 eV, between two couples of nearly degenerate states of leading σ and π symmetries, respectively [Fig. 4(a)]. $(\sqrt{7} \times \sqrt{7})_{\mathrm{I}}$ and $(\sqrt{7} \times \sqrt{7})_{\mathrm{II}}$ silicene exhibit a quasilinear π-like dispersion in the first VB and first CB at K, i.e., a Dirac-cone structure with a tiny band gap below ~0.02 eV [Figs. 4(b) and 4(c)]. The second VB and CB of these superstructures are of dominant σ symmetry. (1×1) silicene has two quasimetallic bands of dominant π character [Fig. 4(d)], whose dispersions resemble the π bands of graphene [68] on a reduced energy scale and with a smaller Fermi velocity [59]. Even in the latter case, the second VB and CB are dominantly σ, however, a $\pi \leftrightarrow \sigma$ inversion has been detected at the crossing points between the first and second VBs and the (avoided) crossing points between the first and second CBs [59].

All these silicene systems have specific high-intensity peaks in their DOS that support electron excitations between the first or second VB and CB near E_F, in a region of the 1stBZ where the bands are quasiflat, and may assist π-like and π-σ plasmon oscillations. The corresponding low-energy vertical transitions, leading to small-momentum EL peaks, are indicated by dashed arrow lines in Figs. 4 and 5.

As a second step of the TDDFT framework, we computed the unperturbed susceptibility of the KS electrons to an energy loss ω and momentum transfer **q** from the incident electron,

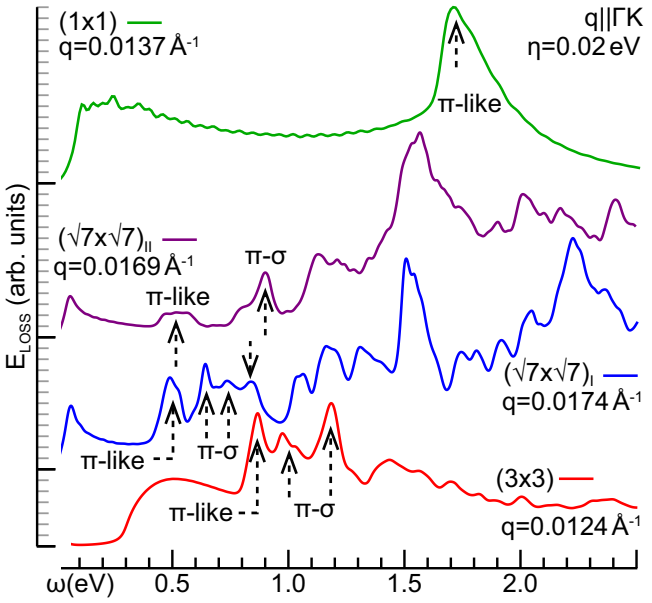

FIG. 5. EL function of (3×3), $(\sqrt{7} \times \sqrt{7})_{\mathrm{I}}$, $(\sqrt{7} \times \sqrt{7})_{\mathrm{II}}$, and (1×1) silicene for $q < 0.02$ Å^{-1} and $\omega < 2.5$ eV, with the lower-energy peaks, associated with transitions close to E_F, being represented by dashed arrow lines (as in Fig. 4).

provided by [69]

$$\chi^0_{\mathbf{GG'}} = \frac{2}{\Omega} \sum_{\mathbf{k},\nu,\nu'} \frac{(f_{\nu\mathbf{k}} - f_{\nu'\mathbf{k+q}}) \rho^{\mathbf{kq}}_{\nu\nu'}(\mathbf{G}) \, \rho^{\mathbf{kq}}_{\nu\nu'}(\mathbf{G'})^*}{\omega + \varepsilon_{\nu\mathbf{k}} - \varepsilon_{\nu'\mathbf{k+q}} + i\eta}. \quad (1)$$

The latter (reported in Hartree atomic units) includes a factor of 2 for the electron spin, the Fermi-Dirac occupations $f_{\nu\mathbf{k}}$ and $f_{\nu\mathbf{k+q}}$ (evaluated at room temperature), a lifetime broadening parameter η (set to 0.02 eV), and the density-density correlation matrix elements $\rho^{\mathbf{kq}}_{\nu\nu'}(\mathbf{G}) = \langle \nu\mathbf{k} | e^{-i(\mathbf{q}+\mathbf{G})\cdot\mathbf{r}} | \nu'\mathbf{k}+\mathbf{q} \rangle$.

The full susceptibility was obtained using the central equation of TDDFT [70], $\chi_{\mathbf{GG'}} = \chi^0_{\mathbf{GG'}} + (\chi^0 v \chi)_{\mathbf{GG'}}$. Working in the RPA, we represented the interaction matrix elements in $\chi_{\mathbf{GG'}}$ by a truncated Coulomb potential, which has been accurately designed to exclude the unphysical interaction between the silicene slab replicas in a broad range of transferred momenta across the whole 1stBZ [71–73].

Accordingly, the inverse permittivity was obtained as $(\epsilon^{-1})_{\mathbf{GG'}} = \delta_{\mathbf{GG'}} + (v\chi)_{\mathbf{GG'}}$ and the EL function was calculated from the macroscopic average $E_{\mathrm{LOSS}} = -\mathrm{Im}[(\epsilon^{-1})_{\mathbf{00}}]$. Nonlocal field effects [74] were included in E_{LOSS} through a dimensional cutoff on the central equation of TDDFT, which we verified to converge by a reduction to a 61×61 matrix equation, including the smallest **G** vectors sorted in length from 0 to ~9.5 Å^{-1}.

In Fig. 5, we compare the theoretical loss spectra of our silicene systems, at fixed small momentum transfers parallel to ΓK in an energy loss range below 2.5 eV. The superstructures present a sequence of low-energy peaks associated with quasivertical electron excitations between the first or second VB and CB, of dominant π or σ character [Figs. 4(a)–4(c)]. Accordingly, the momentum-dependent investigation of Figs. 6(a)–6(c) let us identify two dispersive modes, which we

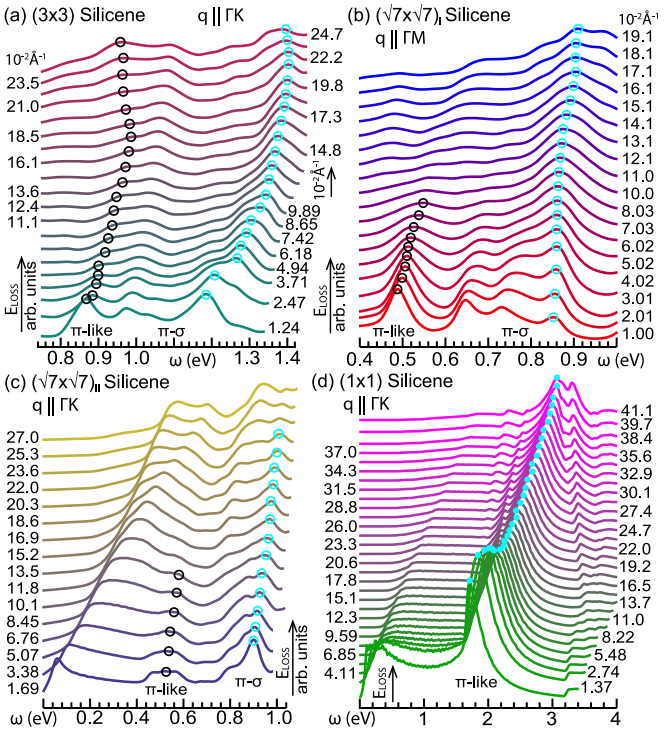

FIG. 6. EL functions of (a) (3×3), (b) $(\sqrt{7} \times \sqrt{7})_{\mathrm{I}}$, (c) $(\sqrt{7} \times \sqrt{7})_{\mathrm{II}}$, and (d) (1×1) silicene along the ΓK [(a), (b), (d)] and ΓM [(c)] directions of the 1$^{\mathrm{st}}$BZs (insets of Fig. 4).

respectively attribute to a π-like plasmon, assisted by first-VB-to-first-CB transitions, and a π-σ plasmon, assisted by second-VB-to-first-CB and first-VB-to-second-CB transitions. Much insight into the latter oscillation in $(\sqrt{7} \times \sqrt{7})_{\mathrm{I}}$ silicene is provided in Sec. B of the Supplemental Material [66].

More importantly, we notice that there is no way that the EL functions of the silicene superstructures can be combined to reproduce the experimental loss spectrum of the mixed phase [curve (iii) in Fig. 3]. Conversely, (1×1) silicene exhibits a broad primary π-like plasmon peak [Figs. 5 and 6(d)], consistent with the EELS spectrum of the mixed phase, which is assisted by first-VB-to-first-CB transitions around the M point and superimposed to secondary one-electron excitation structures. The detailed features of this mode have been carefully addressed in Ref. [59], and are briefly recalled in Sec C of the Supplemental Material [66]. A π-σ mode is also present at energies larger than $\sim$4 eV (Fig. 7).

Of particular significance are then the low-energy features at $\omega = 0.8$–1.3 eV, for (3×3) silicene, and $\omega = 0.4$–0.9 eV, for $(\sqrt{7} \times \sqrt{7})_{\mathrm{I}}$, $(\sqrt{7} \times \sqrt{7})_{\mathrm{II}}$ silicene, because they appear not to be completely erased by the interaction with Ag(111).

Indeed, the experimental loss of the pure $(2\sqrt{3} \times 2\sqrt{3})R30^{\circ}$ phase [spectrum (ii) in Fig. 3] shows a peak, which has some match with the low-energy end of the theoretical loss function of $(\sqrt{7} \times \sqrt{7})_{\mathrm{I}}$ silicene, lying within the energy window of vertical transitions associated with the π-σ plasmon (Figs. 4 and 5).

The interaction with silver destroys the high-energy loss properties of the peeled phase and distorts the low-energy peak, which we ascribe to a hybridized Si-Ag plasmon. This interpretation is confirmed by existing DFT calculations [56]

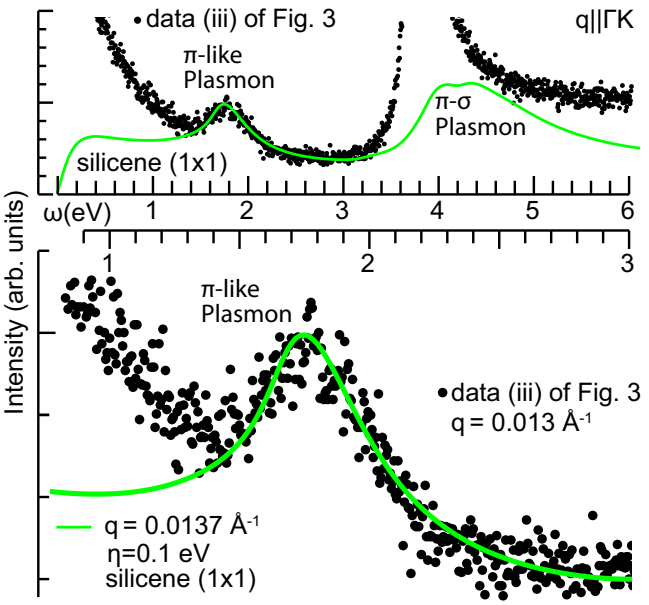

FIG. 7. Experimental loss spectrum (iii) of Fig. 3 and theoretical loss function of (1×1) silicene, where the lowest sampled q value along ΓK is considered with an overall broadening of 0.1 eV to match the experimental resolution.

and validated by our analysis on the $(2\sqrt{3} \times 2\sqrt{3})R30^{\circ}$ phase in Secs. A and B of the Supplemental Material [66], suggesting that the low-energy mode arises due to charge-density oscillations within the silicene and first silver layers and keeps trace of the peeled phase (Figs. S2 and S5 in the Supplemental Material [66]). On the contrary, no signature of an interband plasmon at $\omega = 1.7$–2 eV appears in the theoretical loss spectrum of the silicene superstructures.

A more suggestive result is shown in Fig. 7, where (1×1) silicene calculations are compared with the EL measurements on the coexisting silicene/Ag(111) phases [loss-curve (iii) in Fig. 3]. The excellent agreement, at energy losses below 3 eV, lets us conclude that this morphology indeed presents a dielectric response that matches what is expected for the π-like plasmon of ideal silicene. Also interesting to notice is that the π-σ plasmon of (1×1) silicene may be present as well, though it is hidden by the Ag plasmon of the interface, as verified by comparing the loss spectrum of the mixed phase with that of clean Ag(111) [(i) in Fig. 3].

Hence, the interaction between the pure phases not only weakens the hybridization of Si and Ag states, but also appears to *merge* the different buckling levels of supported silicene into a configuration that resembles that of freestanding silicene. Indeed, the different silicene superstructures are expected to arrange into buckling conformations that mimic that of (1×1) silicene, when their distances, relative to the Ag substrate, are increased above the 2.13–2.16 Å values, predicted for the pure phases. Our DFT calculations on the $(2\sqrt{3} \times 2\sqrt{3})R30^{\circ}$ phase indicate that (1×1) silicene domains begin to form for average Si-Ag distances larger than 3.3 Å (see Fig. S3 in the Supplemental Material [66]). This is the main result of the present study, which awaits further scrutiny, especially regarding the low-q dispersion [75,76] of this π-like mode (see Sec. C of the Supplemental Material [66]).

To summarize our results, we have presented a combined experimental (EELS) and theoretical (TDDFT) approach to show that silicene grown in a mixed phase on Ag(111) preserves at least part of the semimetallic character of its freestanding form, exhibiting an interband π-like plasmon assisted by excitation processes at the M point of the 1stBZ. Such a mode parallels the π plasmon of freestanding graphene [59]. The presence of a π-like plasmon by itself does not allow us to conclude that the silicene overlayer maintains its natural Dirac-cone structure. For example, the interfaces of graphene on the (111) faces of copper and nickel have a well-characterized π plasmon, with the Dirac cone being preserved and destroyed, respectively, by hybridization with the d bands of the supporting metal [77,78]. Nonetheless, in the latter case, the shape, position, and dispersion of the plasmon peak is substantially different from that of freestanding graphene [79], which encourages performing further investigations on mixed-phase morphologies of silicene on silver. A similar approach would help to characterize the first VB and CB of silicene on Au(111) [29], and corroborate the expected Dirac-cone properties of the system.

On the other hand, recent progress on the epitaxial synthesis of pure, single phases of silicene on Ag(111), supported by DFT computations of their electronic properties, indicate that strong hybridization effects make it impractical to separate a silicene structure with a well-defined quasimetallic character. An experimental fingerprint of this phenomenon is the hybridized Si-Ag plasmon, discovered at low energy. Our proposal is then to shift the efforts of making silicene a feasible two-dimensional nanomaterial beyond graphene on the epitaxial growth of silicene in mixed domains.

A.S. acknowledges the computing facilities provided by the CINECA Consortium, within the INF16_npqcd project, under the CINECA-INFN agreement, and the IsC49_PPGRBGI project.

A.S. and A.C. contributed equally to this work.

[1] K. S. Novoselov, A. K. Geim, S. V. Morozov, D. Jiang, Y. Zhang, S. V. Dubonos, I. V. Grigorieva, and A. A. Firsov, Electric field effect in atomically thin carbon films, Science **306**, 666 (2004).

[2] A. Kara, H. Enriquez, A. P. Seitsonen, L. C. Lew Y. Voon, S. Vizzini, B. Aufray, and H. Oughaddou, A review on silicene–New candidate for electronics, Surf. Sci. Rep. **67**, 1 (2012).

[3] M. Houssa, A. Dimoulas, and A. Molle, Silicene: A review of recent experimental and theoretical investigations, J. Phys.: Condens. Matter **27**, 253002 (2015).

[4] S. Cahangirov, H. Sahin, G. Le Lay, and A. Rubio, *Introduction to the Physics of Silicene and other 2D Materials*, Lecture Notes in Physics No. 930 (Springer, Berlin, 2017).

[5] K. Takeda and K. Shiraishi, Theoretical possibility of stage corrugation in Si and Ge analogs of graphite, Phys. Rev. B **50**, 14916 (1994).

[6] G. G. Guzman-Verri and L. C. Lew Yan Voon, Electronic structure of silicon-based nanostructures, Phys. Rev. B **76**, 075131 (2007).

[7] S. Cahangirov, M. Topsakal, E. Akturk, H. Sahin, and S. Ciraci, Two- and One-Dimensional Honeycomb Structures of Silicon and Germanium, Phys. Rev. Lett. **102**, 236804 (2009).

[8] S. Lebègue and O. Eriksson, Electronic structure of two-dimensional crystals from *ab initio* theory, Phys. Rev. B **79**, 115409 (2009).

[9] L. C. Lew Yan Voon, E. Sandberg, R. S. Aga, and A. A. Farajian, Hydrogen compounds of group-IV nanosheets, Appl. Phys. Lett. **97**, 163114 (2010).

[10] C.-C. Liu, W. Feng, and Y. Yao, Quantum Spin Hall Effect in Silicene and Two-Dimensional Germanium, Phys. Rev. Lett. **107**, 076802 (2011).

[11] H. Pan, Z. Li, C.-C. Liu, G. Zhu, Z. Qiao, and Y. Yao, Valley-Polarized Quantum Anomalous Hall Effect in Silicene, Phys. Rev. Lett. **112**, 106802 (2014).

[12] Z. Ni, Q. Liu, K. Tang, J. Zheng, J. Zhou, R. Qin, Z. Gao, D. Yu, and J. Lu, Tunable bandgap in silicene and germanene, Nano Lett. **12**, 113 (2011).

[13] T. H. Osborn, A. A. Farajian, O. V. Pupysheva, R. S. Aga, and L. L. Y. Voon, *Ab initio* simulations of silicene hydrogenation, Chem. Phys. Lett. **511**, 101 (2011).

[14] N. D. Drummond, V. Zólyomi, and V. I. Fal'ko, Electrically tunable band gap in silicene, Phys. Rev. B **85**, 075423 (2012).

[15] H.-R. Chang, J. Zhou, H. Zhang, and Y. Yao, Probing the topological phase transition via density oscillations in silicene and germanene, Phys. Rev. B **89**, 201411 (2014).

[16] C. J. Tabert and E. J. Nicol, Dynamical polarization function, plasmons, and screening in silicene and other buckled honeycomb lattices, Phys. Rev. B **89**, 195410 (2014).

[17] S. Trivedi, A. Srivastava, and R. Kurchania, Silicene and germanene: A first principle study of electronic structure and effect of hydrogenation-passivation, J. Comput. Theor. Nanosci. **11**, 781 (2014).

[18] B. Lalmi, H. Oughaddou, H. Enriquez, A. Kara, S. Vizzini, B. Ealet, and B. Aufray, Epitaxial growth of a silicene sheet, Appl. Phys. Lett. **97**, 223109 (2010).

[19] A. Bhattacharya, S. Bhattacharya, and G. P. Das, Exploring semiconductor substrates for silicene epitaxy, Appl. Phys. Lett. **103**, 123113 (2013).

[20] C. Léandri, H. Oughaddou, B. Aufray, J. M. Gay, G. Le Lay, A. Ranguis, and Y. Garreau, Growth of Si nanostructures on Ag(001), Surf. Sci. **601**, 262 (2007).

[21] A. Kara, C. Léandri, M. E. Dévila, P. De Padova, B. Ealet, H. Oughaddou, B. Aufray, and G. Le Lay, Physics of silicene stripes, J. Supercond. Novel Magn. **22**, 259 (2009).

[22] B. Aufray, A. Kara, S. Vizzini, H. Oughaddou, C. Léandri, B. Ealet, and G. Le Lay, Graphene-like silicon nanoribbons on Ag(110): A possible formation of silicene, Appl. Phys. Lett. **96**, 183102 (2010).

[23] P. De Padova, C. Quaresima, C. Ottaviani, P. M. Sheverdyaeva, P. Moras, C. Carbone, D. Topwal, B. Olivieri, A. Kara, H. Oughaddou, B. Aufray, and G. Le Lay, Evidence of graphene-like electronic signature in silicene nanoribbons, Appl. Phys. Lett. **96**, 261905 (2010).

[24] P. De Padova, P. Perfetti, B. Olivieri, C. Quaresima, C. Ottaviani, and G. Le Lay, 1D graphene-like silicon systems: Silicene nano-ribbons, J. Phys.: Condens. Matter **24**, 223001 (2012).

[25] P. Vogt, P. De Padova, C. Quaresima, J. Avila, E. Frantzeskakis, M. C. Asensio, A. Resta, B. Ealet, and G. Le Lay, Silicene: Compelling Experimental Evidence for Graphenelike Two-Dimensional Silicon, Phys. Rev. Lett. **108**, 155501 (2012).

[26] B. Feng, Z. Ding, S. Meng, Y. Yao, X. He, P. Cheng, L. Chen, and K. Wu, Evidence of silicene in honeycomb structures of silicon on Ag(111), Nano Lett. **12**, 3507 (2012).

[27] A. Fleurence, R. Friedlein, T. Ozaki, H. Kawai, Y. Wang, and Y. Yamada-Takamura, Experimental Evidence for Epitaxial Silicene on Diboride Thin Films, Phys. Rev. Lett. **108**, 245501 (2012).

[28] L. Meng, Y. Wang, L. Zhang, S. Du, R. Wu, L. Li, Y. Zhang, G. Li, H. Zhou, W. A. Hofer, and M. J. Gao, Buckled silicene formation on Ir(111), Nano Lett. **13**, 685 (2013).

[29] S. Sadeddine, H. Enriquez, A. Bendounan, P. K. Das, I. Vobornik, A. Kara, A. J. Mayne, F. Sirotti, G. Dujardin, and H. Oughaddou, Compelling experimental evidence of a Dirac cone in the electronic structure of a 2D silicon layer, Sci. Rep. **7**, 44400 (2017).

[30] C.-L. Lin, R. Arafune, K. Kawahara, N. Tsukahara, E. Minamitani, Y. Kim, N. Takagi, and M. Kawai, Structure of silicene grown on Ag(111), Appl. Phys. Express **5**, 45802 (2012).

[31] H. Jamgotchian, Y. Colignon, N. Hamzaoui, B. Ealet, J. Y. Hoarau, B. Aufray, and J. P. Biberian, Growth of silicene layers on Ag(111): Unexpected effect of the substrate temperature, J. Phys.: Condens. Matter **24**, 172001 (2012).

[32] Z. Majzik, M. R. Tchalala, M. Svec, P. Hapala, H. Enriquez, A. Kara, A. J. Mayne, G. Dujardin, P. Jelinek, and H. Oughaddou, Combined AFM and STM measurements of a silicene sheet grown on the Ag(111) surface, J. Phys.: Condens. Matter **25**, 225301 (2013); H. Liu, J. Gao, and J. Zhao, Silicene on substrates: Interaction mechanism and growth behavior, J. Phys.: Conf. Ser. **491**, 012007 (2014).

[33] C. Grazianettia, D. Chiappe, E. Cinquanta, G. Tallarida, M. Fanciullia, and A. Molle, Exploring the morphological and electronic properties of silicene superstructures, Appl. Surf. Sci. **291**, 109 (2014); Z. L. Liu, M. X. Wang, J. P. Xu, J. F. Ge, G. Le Lay, P. Vogt, D. Qian, C. L. Gao, C. H. Liu, and J. F. Jia, Various atomic structures of monolayer silicene fabricated on Ag(111), New J. Phys. **16**, 075006 (2014).

[34] E. Scalise, E. Cinquanta, M. Houssa, B. van den Broek, D. Chiappe, C. Grazianetti, G. Pourtoisc, B. Ealet, A. Molle, M. Fanciulli, V. V. Afanas'ev, and A. Stesmans, Vibrational properties of epitaxial silicene layers on (111) Ag, Appl. Surf. Sci. **291**, 113 (2014).

[35] P. Moras, T. O. Mentes, P. M. Sheverdyaeva, A. Locatelli, and C. Carbone, Coexistence of multiple silicene phases in silicon grown on Ag(111), J. Phys.: Condens. Matter **26**, 185001 (2014).

[36] H. Enriquez, S. Vizzini, A. Kara, B. Lalmi, and H. Oughaddou, Silicene structures on silver surfaces, J. Phys.: Condens. Matter **24**, 314211 (2012).

[37] R. Arafune, C.-L. Lin, K. Kawahara, M. Kanno, N. Tsukahara, E. Minamitani, Y. Kim, N. Takagi, and M. Kawai, Structural transition of silicene on Ag(111), Surf. Sci. **608**, 297 (2013).

[38] K. Kawahara, T. Shirasawa, R. Arafune, C.-L. Lin, T. Takahashi, M. Kawai, and N. Takagi, Determination of atomic positions in silicene on Ag(111) by low-energy electron diffraction, Surf. Sci. **623**, 25 (2014).

[39] M. R. Tchalala, H. Enriquez, H. Yildirim, A. Kara, A. J. Mayne, G. Dujardin, M. Ait Ali, and H. Oughaddou, Atomic and electronic structures of the $(\sqrt{13} \times \sqrt{13})R13.9^\circ$ of silicene sheet on Ag(111), Appl. Surf. Sci. **303**, 61 (2014).

[40] C.-L. Lin, R. Arafune, K. Kawahara, M. Kanno, N. Tsukahara, E. Minamitani, Y. Kim, M. Kawai, and N. Takagi, Substrate-Induced Symmetry Breaking in Silicene, Phys. Rev. Lett. **110**, 076801 (2013).

[41] Z.-L. Liu, M.-X. Wang, C. Liu, J.-F. Jia, P. Vogt, C. Quaresima, C. Ottaviani, B. Olivieri, P. De Padova, and G. Le Lay, The fate of the $(2\sqrt{3} \times 2\sqrt{3})R30^\circ$ silicene phase on Ag(111), APL Mater. **2**, 092513 (2014).

[42] H. Enriquez, A. Kara, A. J. Mayne, G. Dujardin, H. Jamgotchian, B. Aufray, and H. Oughaddou, Atomic structure of the $(2\sqrt{3} \times 2\sqrt{3})R30^\circ$ of silicene on Ag(111) surface, J. Phys.: Conf. Ser. **491**, 012004 (2014).

[43] J. Avila, P. De Padova, S. Cho, I. Colambo, S. Lorcy, C. Quaresima, P. Vogt, A. Resta, G. Le Lay, and M. C. Asensio, Presence of gapped silicene-derived band in the prototypical (3×3) silicene phase on silver (111) surfaces, J. Phys.: Condens. Matter **25**, 262001 (2013).

[44] A. Resta, T. Leoni, C. Barth, A. Ranguis, C. Becker, T. Bruhn, P. Vogt, and G. Le Lay, Atomic structures of silicene layers grown on Ag(111): Scanning tunneling microscopy and noncontact atomic force microscopy observations, Sci. Rep. **3**, 2399 (2013).

[45] H. Jamgotchian, Y. Colignon, B. Ealet, B. Parditka, J.-Y. Hoarau, C. Girardeaux, B. Aufray, and J.-P. Bibérian, Silicene on Ag(111): Domains and local defects of the observed superstructures, J. Phys.: Conf. Ser. **491**, 012001 (2014).

[46] L. Chen, C.-C. Liu, B. Feng, X. He, P. Cheng, Z. Ding, S. Meng, Y. Yao, and K. Wu, Evidence for Dirac Fermions in a Honeycomb Lattice Based on Silicon, Phys. Rev. Lett. **109**, 056804 (2012).

[47] Z.-X. Guo, S. Furuya, J. I. Iwata, and A. Oshiyama, Absence and presence of Dirac electrons in silicene on substrates, Phys. Rev. B **87**, 235435 (2013).

[48] Z.-X. Guo, S. Furuya, J. Iwata, and A. Oshiyama, Absence of Dirac Electrons in Silicene on Ag(111) Surfaces, J. Phys. Soc. Jpn. **82**, 063714 (2013).

[49] P. Pflugradt, L. Matthes, and F. Bechstedt, Silicene-derived phases on Ag(111) substrate versus coverage: *Ab initio* studies, Phys. Rev. B **89**, 035403 (2014).

[50] F. Ronci, G. Serrano, P. Gori, A. Cricenti, and S. Colonna, Silicon-induced faceting at the Ag(110) surface, Phys. Rev. B **89**, 115437 (2014); M. Satta, S. Colonna, R. Flammini, A. Cricenti, and F. Ronci, Silicon reactivity at the Ag(111) surface, Phys. Lett. B **115**, 026102 (2015).

[51] P. De Padova, A. Generosi, B. Paci, C. Ottaviani, C. Quaresima, B. Olivieri, E. Salomon, T. Angot, and G. Le Lay, Multilayer silicene: clear evidence, 2D Mater. **3**, 031011 (2016).

[52] A. Acun, B. Poelsema, H. J. W. Zandvliet, and R. van Gastel, The instability of silicene on Ag(111), Appl. Phys. Lett. **103**, 263119 (2013).

[53] D. Tsoutsou, E. Xenogiannopoulou, E. Golias, P. Tsipas, and A. Dimoulas, Evidence for hybrid surface metallic band in (4×4) silicene on Ag(111), Appl. Phys. Lett. **103**, 231604 (2013).

[54] Y.-P. Wang and H.-P. Cheng, Does silicene on Ag(111) have a Dirac cone? Phys. Rev. B **87**, 245430 (2013).

[55] S. K. Mahatha, P. Moras, V. Bellini, P. M. Sheverdyaeva, C. Struzzi, L. Petaccia, and C. Carbone, Silicene on Ag(111): A honeycomb lattice without Dirac bands, Phys. Rev. B **89**, 201416 (2014).

[56] P. M. Sheverdyaeva, S. K. Mahatha, P. Moras, L. Petaccia, G. Fratesi, G. Onida, and C. Carbone, Electronic states of silicene allotropes on Ag(111), ACS Nano **11**, 975 (2017).

[57] Y. Feng *et al.*, Direct evidence of interaction-induced Dirac cones in a monolayer silicene/Ag(111) system, Proc. Natl. Acad. Sci. USA **113**, 14656 (2016).

[58] R. Quhe, Y. Yuan, J. Zheng, Y. Wang, Z. Ni, J. Shi, D. Yu, J. Yang, and J. Lu, Does the Dirac cone exist in silicene on metal substrates? Sci. Rep. **4**, 5476 (2014).

[59] C. Vacacela Gomez, M. Pisarra, M. Gravina, P. Riccardi, and A. Sindona, Plasmon properties and hybridization effects in silicene, Phys. Rev. B **95**, 085419 (2017).

[60] M. Petersilka, U. J. Gossmann, and E. K. U. Gross, Excitation Energies from Time-Dependent Density-Functional Theory, Phys. Rev. Lett. **76**, 1212 (1996).

[61] X. Gonze, B. Amadon, P.-M. Anglade, J.-M. Beuken, F. Bottin, P. Boulanger, F. Bruneval, D. Caliste, R. Caracas, M. Cote *et al.*, ABINIT: First-principles approach to material and nanosystem properties, Comput. Phys. Commun. **180**, 2582 (2009).

[62] P. Hohenberg and W. Kohn, Inhomogeneous electron gas, Phys. Rev. **136**, B864 (1964).

[63] J. P. Perdew, K. Burke, and M. Ernzerhof, Generalized Gradient Approximation Made Simple, Phys. Rev. Lett. **77**, 3865 (1996); Generalized Gradient Approximation Made Simple, *ibid.* **78**, 1396(E) (1997).

[64] N. Troullier and J. L. Martins, Efficient pseudopotentials for plane-wave calculations, Phys. Rev. B **43**, 1993 (1991).

[65] H. J. Monkhorst and J. D. Pack, Special points for Brillouin-zone integrations, Phys. Rev. B **13**, 5188 (1976).

[66] See Supplemental Material at http://link.aps.org/supplemental/10.1103/PhysRevB.97.041401 for (A) electronic structure of the $(2\sqrt{3} \times 2\sqrt{3})R30^\circ$ phase, (B) loss function of $(\sqrt{7} \times \sqrt{7})_\mathrm{I}$ silicene and EELS spectrum of the $(2\sqrt{3} \times 2\sqrt{3})R30^\circ$ phase, and (C) π-like plasmon mode of (1×1) silicene vs EELS spectra of the mixed phase.

[67] J. P. Perdew and A. Zunger, Self-interaction correction to density-functional approximations for many-electron systems, Phys. Rev. B **23**, 5048 (1981).

[68] A. Sindona, M. Pisarra, C. Vacacela Gomez, P. Riccardi, G. Falcone, and S. Bellucci, Calibration of the fine-structure constant of graphene by time-dependent density-functional theory, Phys. Rev. B **96**, 201408(R) (2017).

[69] S. L. Adler, Quantum theory of the dielectric constant in real solids, Phys. Rev. **126**, 413 (1962); N. Wiser, Dielectric constant with local field effects included, *ibid.* **129**, 62 (1963).

[70] G. Onida, L. Reining, and A. Rubio, Electronic excitations: Density-functional versus many-body Green's-function approaches, Rev. Mod. Phys. **74**, 601 (2002).

[71] V. Despoja, K. Dekanić, M. Šunjić, and L. Marušić, *Ab initio* study of energy loss and wake potential in the vicinity of a graphene monolayer, Phys. Rev. B **86**, 165419 (2012).

[72] M. Pisarra, A. Sindona, P. Riccardi, V. M. Silkin, and J. M. Pitarke, Acoustic plasmons in extrinsic free-standing graphene, New J. Phys. **16**, 083003 (2014).

[73] C. Vacacela Gomez, M. Pisarra, M. Gravina, J. M. Pitarke, and A. Sindona, Plasmon Modes of Graphene Nanoribbons with Periodic Planar Arrangements, Phys. Rev. Lett. **117**, 116801 (2016).

[74] C. Kramberger, R. Hambach, C. Giorgetti, M. H. Rümmeli, M. Knupfer, J. Fink, B. Büchner, L. Reining, E. Einarsson, S. Maruyama, F. Sottile, K. Hannewald, V. Olevano, A. G. Marinopoulos, and T. Pichler, Linear Plasmon Dispersion in Single-Wall Carbon Nanotubes and the Collective Excitation Spectrum of Graphene, Phys. Rev. Lett. **100**, 196803 (2008).

[75] V. U. Nazarov, Multipole surface plasmon excitation enhancement in metals, Phys. Rev. B **59**, 9866 (1999); A. Sindona *et al.*, Many body shake up in x-ray photoemission from bundles of lithium-intercalated single-walled carbon nanotubes, Surf. Sci. **601**, 2805 (2007); P. Riccardi *et al.*, Bulk and surface plasmon excitation in the interaction of He^+ with Mg surfaces, Nucl. Instrum. Methods Phys. Res., Sect. B **212**, 339 (2003); A. Sindona, S. A. Rudi, S. Maletta, R. A. Baragiola, G. Falcone, and P. Riccardi, Auger electron emission from metals induced by low energy ion bombardment: Effect of the band structure and Fermi edge singularity, Surf. Sci. **601**, 1205 (2007).

[76] A. Politano, C. Lamuta, and G. Chiarello, Cutting a Gordian knot: Dispersion of plasmonic modes in Bi_2Se_3 topological insulator, Appl. Phys. Lett. **110**, 211601 (2017).

[77] A. V. Generalov and Y. S. Dedkov, EELS study of the epitaxial graphene/Ni(111) and graphene/Au/Ni(111) systems, Carbon **50**, 183 (2012).

[78] A. Cupolillo, N. Ligato, and L. S. Caputi, Two-dimensional character of the interface π plasmon in epitaxial graphene on Ni(111), Carbon **50**, 2588 (2012); M. Pisarra, P. Riccardi, A. Cupolillo, A. Sindona, and L. S. Caputi, Studies of electron emission in the interaction of electrons with graphene on Ni(111) surface, Nanosci. Nanotechnol. Lett. **4**, 1100 (2012); M. Pisarra, P. Riccardi, A. Sindona, A. Cupolillo, N. Ligato, C. Giallombardo, and L. Caputi, Probing graphene interfaces with secondary electrons, Carbon **77**, 796 (2014); A. Cupolillo, M. Pisarra, A. Sindona, M. Commisso, and P. Riccardi, Electron excitation in the interaction of slow ions and electrons with metals and monolayer graphite on Ni(111) surfaces, Vacuum **84**, 1029 (2010); M. Commisso, A. Bonanno, A. Oliva, M. Camarca, F. Xu, P. Riccardi, and R. A. Baragiola, Plasmon excitation and electron promotion in the interaction of slow Na^+ ions with Al surfaces, Nucl. Instrum. Methods Phys. Res., Sect. B **230**, 438 (2005).

[79] T. Eberlein, U. Bangert, R. R. Nair, R. Jones, M. Gass, A. L. Bleloch, K. S. Novoselov, A. Geim, and P. R. Briddon, Plasmon spectroscopy of free-standing graphene films, Phys. Rev. B **77**, 233406 (2008).